Green Chemistry

Tailorable cellulose II nanocrystals (CNC II) prepared in mildly acidic lithium bromide trihydrate (MALBTH)

Journal:	*Green Chemistry*
Manuscript ID	GC-ART-01-2021-000145.R2
Article Type:	Paper
Date Submitted by the Author:	11-Mar-2021
Complete List of Authors:	Li, Ning; Dalian Institute of Chemical Physics, Bian, Huiyang; Nanjing Forestry University, Zhu, JunYong; US Forest Service, Forest Products Laboratory, Ciesielski, Peter; National Renewable Energy Laboratory, Biosciences Center Pan, Xuejun; University of Wisconsin-Madison, Biological Systems Engineering

Tailorable cellulose II nanocrystals (CNC II) prepared in mildly acidic lithium bromide trihydrate (MALBTH)

Ning Li[1,†], Huiyang Bian[2,3], J.Y. Zhu[3], Peter N. Ciesielski[4], Xuejun Pan[1,]*

1. Department of Biological Systems Engineering, University of Wisconsin-Madison, Madison, WI 53706, USA

2. Jiangsu Co-Innovation Center of Efficient Processing and Utilization of Forest Resources, Nanjing Forestry University, Nanjing, JS 210037, China

3. Forest Products Laboratory, U.S. Forest Service, U.S. Department of Agriculture, Madison, WI 53726, USA

4. Bioscience Center, National Renewable Energy Laboratory, Golden, CO 80401, USA

†. Present address: State Key Laboratory of Catalysis (SKLC), Dalian National Laboratory for Clean Energy (DNL), Dalian Institute of Chemical Physics (DICP), Chinese Academy of Sciences, Dalian 116023, China

*Corresponding Author: Tel. +1-608-2624951; Fax +1-608-2621228; E-mail xpan@wisc.edu

Abstract

Preparing cellulose II nanocrystals (CNC II) requires a polymorph transformation of natural cellulose I feedstocks. The transformation is usually achieved via a process such as mercerization or dissolution-regeneration. This study demonstrated a new method to prepare CNC II directly from bleached kraft pulp (BKP, a commercially available cellulose I feedstock) in a mildly acidic lithium bromide trihydrate (MALBTH) system, a concentrated (~61 wt%) solution of LiBr in water with a very low concentration (2.5 mM) of sulfuric acid. First, the BKP was treated in the

MALBTH system to generate a cellulose II hydrolysis solid residue (CHR) with a yield of 64-86%, during which the selective hydrolysis of disordered cellulose and the polymorph transformation were completed simultaneously. Then, subsequent oxidation of the CHR by ammonium persulfate (APS, 0.1-0.6 M) resulted in the CNC II with high yield (up to 62%), high crystallinity (over 90%), rich surface carboxyl group (0.3-1.2 mmol/g cellulose), excellent colloidal stability (up to -59 mV zeta potential), and high thermal stability. The CNC II had a tunable length (10-200 nm), determined by the conditions of the MALBTH hydrolysis and the APS oxidation, but similar lateral dimension (8-10 nm). The characterization of the CHR with wide-angle X-ray diffraction and Fourier transform infrared spectroscopy verified the polymorph transformation from cellulose I to II during the MALBTH treatment. The swelling of the BKP in the MALBTH enabled cellulose crystallites to slide and reassemble, which completed the rearrangement of cellulose chains from parallel to anti-parallel conformation (polymorph transformation from cellulose I to II). This study provided an efficient and green method to produce cellulose II nanocrystals with controllable aspect ratios via the simultaneous hydrolysis and polymorph transformation of cellulose I feedstocks.

Keywords: Polymorph transformation; molten salt hydrate; nanocellulose; ammonium persulfate oxidation; disordered cellulose hydrolysis

Introduction

Harnessing cellulose (the most abundant biopolymer, ~1.5×10^{12} ton/year) has been constantly pursued[1-3] in merits of renewability, sustainability, biodegradability, and non-toxicity.[4, 5] Traditional cellulosic feedstocks (e.g., cotton and wood logs), composed of hierarchical fiber units

in tens of micron, are either utilized to produce textiles and construction materials, or processed and purified after chemical and mechanical treatments into individual cellulosic fibers for manufacturing paper products and cellulose derivatives. Alternatively, the cellulose fibers can be further downsized to isolate the elementary nanocellulose particles (exhibiting at least one nanoscale dimension), rendering performance-bonus to cellulosic materials (such as improved optical transparency, high surface area, colloidal stability, enhanced surface reactivity, mechanical strength, and barrier property).[3, 4, 6, 7] Enormous efforts have been made to exploit the potential of nanocellulose for biomedical engineering, polymer reinforcement, environmental treatment, energy harvesting/storage, food packaging, etc.[8-10] Depending on the specific applications, cellulose nanomaterials can be either dispersed as 1-dimension individual particles for their excellent interfacial properties and surface chemical reactivity, casted to 2-dimensional films for its flexibility and strength, incorporated into polymer matrices as a strengthening agent, or molded into 3-dimensional hydrogels and aerogels for its porosity and mechanical properties.[8]

Producing cellulose nanocrystal (CNC) usually involves acidic hydrolysis of the cellulosic feedstocks to rupture and remove the disordered regions of cellulose. The hydrolysis conditions, especially the acid type and concentration, play a critical role in the CNC preparation. Concentrated sulfuric acid (e.g., 64%) has been extensively employed due to its excellent ability to swell cellulose fibers and selective hydrolysis of disordered cellulose.[11-13] To improve the dispersibility of cellulose nanoparticles in an aqueous solution, the surface of the nanoparticles needs to be charged, usually negatively, via oxidation,[14, 15], carboxylation,[16] and sulfation reactions, with the latter occurring naturally during sulfuric acid hydrolysis. Other concentrated strong acids such as hydrochloride acid (6M), phosphoric acids (10.7 M), as well as concentrated weak acids such as oxalic acid (50-70%) and maleic acid, have also been used for the preparation

of cellulose nanocrystals.[16-18]

The CNC produced from cellulose fibers through acid hydrolysis described above retains the cellulose I polymorph of native cellulose, which usually has a high aspect ratio (30-100) and is excellent to produce strong and flexible films and reinforced composite materials. The CNC with a low aspect ratio, as well-dispersed 1D particles, could be beneficial in applications such as Pickering emulsifiers, drug/catalyst carriers, and dispersants due to the high interfacial surface coverage as well as abundant surface functional groups.[19-21] However, the low-aspect-ratio CNC was rarely available and difficult to prepare in cellulose I form because the recalcitrant cellulose I crystallites are difficult to deconstruct below their persistence length using mechanical disintegration.[22]

A feasible route to produce the CNCs with small and tunable aspect ratios and particle sizes is to artificially modify (reduce) the size of cellulose crystallites during the polymorph transformation from cellulose I (paralleled chain conformation) to cellulose II (anti-paralleled chain conformation) by tuning treatment conditions. The polymorph transformation can be accomplished via either the mercerization treatment using concentrated sodium hydroxide or dissolution/regeneration processes using a cellulose solvent such as N-methylmorpholine N-oxide (NMMO) or ionic liquids before acid hydrolysis.[23-25] These processes require multiple operations and/or involve costly and toxic/caustic solvents that have poor compatibility with the subsequent operation of cellulose hydrolysis. It was reported that concentrated H_2SO_4 (66%) showed a pseudo-mercerization performance in polymorph transformation, but the treatment conditions fell in a narrow range and varied among different labs.[21, 26] Recently, lithium bromide molten salt hydrate ($LiBr{\cdot}3H_2O$, a LiBr solution in water at a concentration of ~61%) has been identified as an effective solvent for cellulose swelling and dissolution.[27-31] The LBTH is also a green and

recyclable solvent without regulated environmental hazards and risks.[31] Herein, adopting the LiBr trihydrate system, a facile process was designed to prepare cellulose II nanocrystal (CNC II) from a commercial bleached kraft pulp (BKP, cellulose I polymorph). The proposed mildly acidic lithium bromide trihydrate (MALBTH) could achieve selective hydrolysis of disordered cellulose and the polymorph transformation of cellulose simultaneously under swelling conditions. The cellulose II nanocrystal (CNC II) was then modified by diluted ammonia persulfate for easy mechanical disintegration. The resultant CNC II had tunable aspect ratios and surface changes, dependent on the hydrolysis and oxidation conditions.

Experimental

Cellulose feedstock

A commercial bleached kraft pulp (BKP) from eucalyptus was used as feedstock. The pulp board was immersed in deionized (DI) water overnight and mechanically disintegrated into individual fibers. The fiber slurry was concentrated to ~10 wt% and then lyophilized for downstream treatments. The chemical composition of the BKP included glucan (86.7 ± 0.4%) and xylan (11.4 ± 0.2%). The average degree of polymerization (*DP*) of the BKP was 603, determined using the method described below.

Mildly acidic lithium bromide trihydrate (MALBTH) treatment of cellulose

The BKP was suspended in 61% LiBr solution (a solid-to-liquid ratio 1:10, w/v) in a 40-mL glass vial with a sealed cap and a magnetic stir-bar at 100 °C for 45 min to let cellulose fibers fully swell. Then, acid (H_2SO_4, 2.5 mM in the LiBr solution) was added to conduct the mild hydrolysis of cellulose at 100 °C for 10-60 min. The hydrolysis was quenched by dilution with DI water to yield regenerated ivory cellulose hydrolysis solid residue (CHR). The mixture was centrifuged at

4500 rpm for 25 min at 4 °C and then washed three times with DI water. The suspension (approximately at 1 wt% CHR) was transferred to a sealed dialysis tube (12,000 Da molecular weight cutoff) and immersed in a large amount of DI water for 72 h. The yield of CHR was gravimetrically determined based on the initial cellulose content in BKP. The monosaccharides released from BKP during the hydrolysis were quantified using high-performance anion-exchange chromatography (HPAEC) on an ICS-3000 system (Dionex, Sunnyvale, CA) equipped with a pulsed amperometric detector and a 250 mm × 4 mm (length × inner diameter) CarboPac PA1 column (Thermo Scientific, Sunnyvale, CA) at 30 °C. The eluent was fed at a flow rate of 0.7 mL/min, according to the following gradient: 0-25 min, 100% water; 25.1-35 min, 30% water and 70% 0.1 M NaOH; and 35.1-40 min, 100% water. Post-column eluent of 0.5 M NaOH at a flow rate of 0.3 mL/min was used to ensure baseline stability and detector sensitivity.[32]

Preparation of oxidized CNC II (ox-CNC II) by APS oxidation

The ox-CNC II was prepared by oxidizing the CHR with ammonium persulfate (APS, 0.1-0.6 M) at 60 °C for 6-24 h. After APS oxidation, the cellulose residue was collected by centrifugation and further washed with DI water. When the supernatant turned turbid after centrifugation, the whole mixture was transferred to a sealed dialysis tube in DI water and dialyzed for 72 h. The ox-CNC II was then disintegrated using an ultra-sonicator (Sonics Vibra Cell, Newton, CT) at 80% amplitude. The yield of ox-CNC (in the supernatant after centrifugation) was measured gravimetrically and calculated based on the cellulose content in the original BKP.

Wide-angle X-ray diffraction (WAXD) measurement

WAXD measurement was conducted using an X-ray diffractometer (Bruker D8 Discover diffractometer) with Cu-Kα micro X-ray (wavelength 1.5418 Å) and a Vantec 500 area detector. The sample was compressed to a flat cellulose pad (thickness: ~1 mm) and analyzed in a step-scan

mode with 2θ angle ranging from 5° to 55°. The Segal crystallinity index (*CrI*) was calculated using the experimental diffraction patterns after background subtraction following Eq. 1. [29]

$$CrI(\%) = \frac{I_{c+a} - I_a}{I_{c+a}} \times 100 \quad (1)$$

where I_{c+a} is the intensity corresponding to the (200) peak of cellulose Iβ at 2θ 22.7° or the (020) peak of cellulose II at 2θ 21.8°; I_a is the intensity corresponding to the disordered peaks of cellulose Iβ at 2θ 18° or cellulose II at 2θ 16°.

The diffraction pattern was deconvoluted using the Origin 2016 software (OriginLab Corp.) by Gaussian function. The *CrI′* was calculated from the percentage of the areas assigned to crystalline peaks to the areas of all the peaks.

The average size of cellulose crystallites (*d*, nm) perpendicular to the corresponding lattice plane of the diffraction peak was estimated by the Scherrer equation (Eq. 2).[30]

$$d = \frac{K\lambda}{\beta \cos\theta} \quad (2)$$

where *K* denotes the Scherrer constant (0.9); λ denotes the radiation wavelength of the X-ray (0.15418 nm); β denotes the full width at half maximum (FWHM) of the diffraction peak in radians; and θ denotes the Bragg angle of the diffraction peak.

Diffraction simulation

The simulated diffraction patterns of the ideal cellulose Iβ and cellulose II crystallites were obtained using the Mercury 3.9 program (The Cambridge Crystallographic Data Centre, UK).[33] The coordinates of the asymmetric crystal units of both cellulose polymorphs were adopted from Condon et al.[34] The input FWHM was set to be 1.0° (2θ, 0.0174 radians).

Polarized optical microscope (POM)

The morphology of the wetted BKP and CHR samples was monitored using a Motic microscope equipped with two crossed polarizers in reflection mode. The images were recorded via a Q-imaging G3-go camera.

Transmission electron microscopy (TEM)

The dimensions (both length and width) of ox-CNC II were characterized using a Tecnai G2 TF12 TEM (FEI, Hillsboro, OR) with a four mega-pixel GatanUltra Scan 1000 camera. A drop of diluted suspension (0.04 wt% the ox-CNC II in water) was gently loaded on a freshly glow-discharged carbon-coated (5-6 nm in thickness) copper grid (VWR, 300 mesh). After 5 min, the excess liquid was blotted away, and the grid was then covered with 5 μL of 1% aqueous uranyl acetate (negative staining reagent, Sigma-Aldrich) for 2 min. After removing the extra solution, the sample was dried under vacuum before the morphology imaging.

Atomic force microscopy (AFM)

The thickness of ox-CNC II was determined using an AFM Workshop system (Signal Hill, CA). Diluted samples (0.005%) were dropped on freshly peeled mica slices and air-dried overnight at room temperature. AFM scanning was operated in a tapping mode with a resonance frequency in the range of 160-225 kHz and height topographies were analyzed using Gwyddion imaging analysis software (Department of Nanometrol, Czech Metrology Institute, Czech Republic).

Scanning electron microscopy (SEM)

Morphology of BKP fibers and hydrolysis residues was observed by field emission scanning electron microscopy (FE-SEM, Leo Co., Oberkochen, Germany). To prepare SEM samples, a drop of cellulose suspension after solvent exchange by *t*-butanol was placed on a clean aluminum foil. Dried under vacuum, the foil was firmly attached on an aluminum mount by conductive tape and

coated with a thin layer of Au. The SEM images were recorded by an in-lens detector at 3.0 kV accelerating voltage and 4-5 mm working distance.

Dynamic light scattering (DLS) and zeta potential analyses

The ox-CNC II suspension (0.1 wt%) was measured using a DLS analyzer (Nanobrook Omni, Holtsville, NY) at a 90° scattering angle. The resultant hydrodynamic diameter was an average of 5 continuous measures. It provided a rough estimation of nanoparticle size since scattering analysis using the Stokes-Einstein equation.

The interface zeta potential of the ox-CNC II was determined using a phase analysis light scattering (PALS) potential analyzer (NanoBrook, Holtsville, NY) and fitted to the Smoluchowski model. The zeta potential value was read after the accumulation of 30 data cycles and the result was an average of triplicate measures.

Carboxyl group content

Electric conductivity titration was conducted to determine the COOH content of the ox-CNC II. The ox-CNC II suspension (50 mg in dry weight) was mixed with 10 mL of 0.01 M HCl for 5 min and then titrated against 0.01 M of standard NaOH. The consumption of NaOH (mL) by weak carboxylic acid was obtained from the resultant titration curves (Figure S1). Then the carboxyl content (X_c, mmol/g) was calculated following Eq. 3.

$$X_c = \frac{c \times (V_2 - V_1)}{m} \quad (3)$$

where c (mol/L) is the concentration of the standard NaOH solution; V_1 and V_2 (mL) are the volumes of the standard NaOH solution at the inflection points of the titration curve; and m (g), is the oven-dry weight of the ox-CNC II.

Degree of polymerization (*DP*)

DP of cellulose was estimated by a capillary viscometer method following the TAPPI T230 om-

08 procedure. Cellulose samples (0.1 g) were dispersed in 10 mL DI water and subsequently dissolved in 20 mL of 0.5 M cupriethylenediamine (CED) for 30 min. The kinematic viscosity of the solutions equilibrated to 25.0 °C was measured using a Cannon-Fenske capillary viscometer to yield the corresponding intrinsic viscosities ([η]c, mL/g). The *DP* value was calculated from Eq. 4.[35]

$$DP^{0.905} = 0.75[\eta] \quad (4)$$

where the constants of 0.905 and 0.75 are from the empirical values for the polymer-solvent system. It should be mentioned that Eq 4 is empirical and averaged, so the *DP* value from the viscosity measurement may not reflect the DP of individual cellulose chains.

Attenuated total reflectance (ATR) - Fourier transform infrared (FTIR) spectroscopic analysis

The CHR and the ox-CNC II samples were analyzed by ATR-FTIR spectroscopy (PerkinElmer Spectrum 100, Hopkinton, MA). Each measurement was recorded by 64 scans at 4 cm^{-1} resolution.

Hydrogen-deuterium exchange

Hydrogen-deuterium exchange (a facile approach to probe the accessibility of cellulose to water) was conducted in the MALBTH system. Under the conditions analogous to CHR preparation, BKP fibers (10%, w/v loading) were either fully swelled in $LiBr{\cdot}3D_2O$ at 100 °C for 60 min or partially hydrolyzed in $LiBr{\cdot}3D_2O$ (containing 2.5 mM H_2SO_4, deuterated MALBTH) at 100 °C for 30 min. After immersion in an ice water bath for 10 min, the mixture underwent a 10-fold dilution with D_2O and was subsequently washed by either D_2O or H_2O. In the experimental control, BKP was treated in D_2O at 100 °C for 60 min. All samples were dried in an isothermal oven at 105 °C for 12 h, cooled down in a moisture-free desiccator, and immediately analyzed using ATR-FTIR with minimal exposure to ambient moisture. The baseline-correction, peak deconvolution, and

integration were processed using the Origin 2016 software (OriginLab Corp.)

Thermogravimetric analysis (TGA)

The thermal stability was determined by a Q500 thermogravimetric analyzer (TA Instruments, Wilmington, DE). Cellulose samples (4.0 mg) were heated from 30 to 600 °C at a rate of 10 °C/min under a flow of nitrogen at 20 mL/min.

Results and discussion

Controlled hydrolysis of BKP in the MALBTH

The BKP in this study was industrially manufactured from hardwood (eucalyptus) by kraft pulping. Lignin had been extensively removed during the pulping and bleaching. The BKP fibers are composed dominantly of cellulose (~87%) along with a small amount of hemicellulose (~11%), as indicated by composition analysis (the Klason method). In our previous study[36], prompt dissolution and hydrolysis of cellulose in acidic lithium bromide trihydrate (ALBTH) was described, when sufficient acid concentration and temperature were provided. With these observations, it was hypothesized that if cellulose fibers were swelled in the LiBr solution under mild temperature (e.g., 100 °C) but remained in a solid-state (undissolved), and then acid was introduced at a very low concentration (e.g., 5 mM H^+) to selectively hydrolyze disordered cellulose and hemicelluloses under the swelling conditions, it would be possible to prepare CNC II from the BKP via simultaneous hydrolysis of disordered cellulose and polymorph transformation in the mildly acidic lithium bromide trihydrate (MALBTH) system.

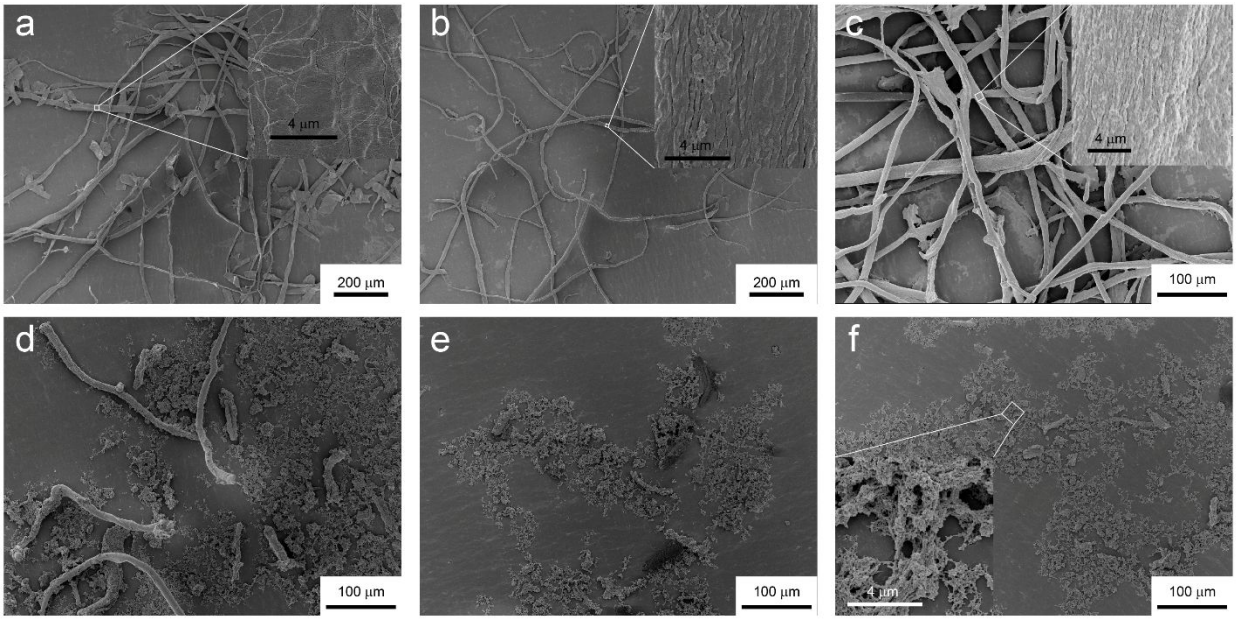

Figure 1. SEM images of the original BKP(a), swelled BKP in LBTH (b), CHR after the MALBTH treatment (c, 10 min; d, 20 min; e, 30 min; f, 60 min).

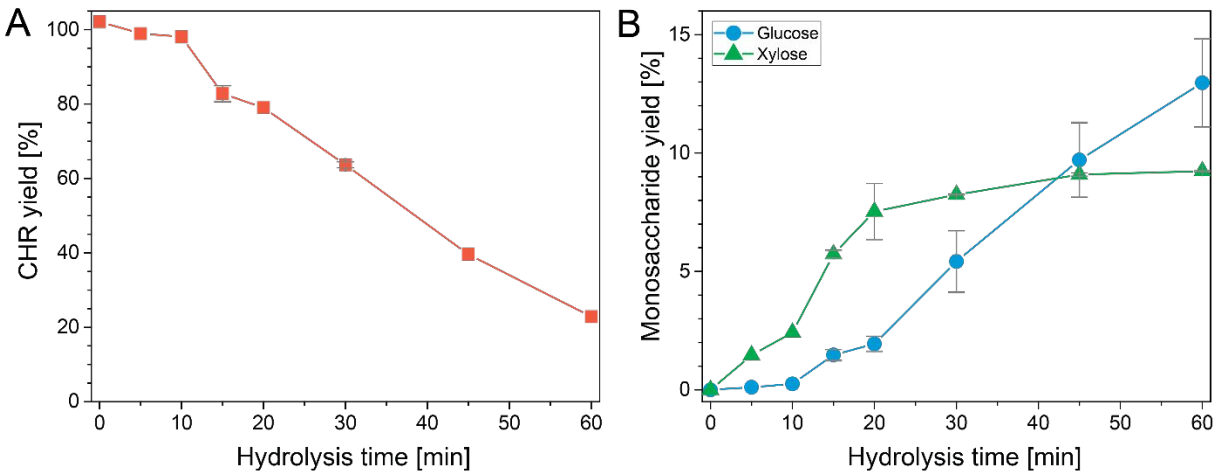

Figure 2. Yields of CHR (A), glucose, and xylose (B) from BKP as a function of treatment time in the MALBTH.

The macroscopic structures and morphology of the BKP during the treatment in the MALBTH were observed using SEM (Figure 1, dry samples) and POM (Figure S2, wet samples), respectively. The original BKP consisted mainly of cellulose fiber cells with a small number of

parenchyma cells (Figure 1a). After the pretreatment in lithium bromide trihydrate (LBTH) without acid, the parenchyma cells were almost invisible. These thin-wall cells were likely destructed and dissolved in the LBTH. The cellulose fibers remained mostly intact in the length dimension (Figure 1b and S2B). Compared with the smooth surface of the original BKP, a wrinkled surface was observed after the LBTH pretreatment (amplified insets in Figure 1a and 1b), which was presumably caused by the drying-induced shrinkage of the swelled fibers when preparing the SEM sample. Similar surface topology was also observed during the mercerization process.[37] In the first 10 min of the MLBTH treatment, macroscopic structures of the fibers were mostly preserved, and the surface morphology resembled that carried over from the LBTH pretreatment, though fractures or tiny holes appeared, possibly due to acidic corrosion. This observation was indicative of cellulose hydrolysis inside the fiber cell wall under swelling conditions. Extending the treatment time in the MALBTH, the BKP fibers were remarkably cut along the length dimension. The average length of the fiber fragments in average was shorter than 500 and 100 μm in length after 20 and 30 min, respectively. The cellulose particles from the fiber destruction, especially those after extensive treatment in the MALBTH, showed nano-scale porous structures (the inset of Figure 1f), which were distinct from those isolated by extensive enzymatic hydrolysis or concentrated acid hydrolysis of cellulose.[38-40]

Table 1. Effect of the treatment time in the MALBTH on crystallinity, crystalline dimension, and *DP* of the CHR from the BKP

Sample	CrI (%)	Crystallite size (nm)			*DP*
		(1-10)	(110)	(200)/(020)	
CHR	75.1	5.8	3.0	5.6	603
0 min	62.9	5.7	2.8	3.4	553
5 min	72.3	5.8	2.7	2.9	208
10 min	73.2	6.2	2.7	3.1	139
15 min	75.3	6.0	3.2	4.1	79

20 min	79.2	6.4	3.4	4.2	67
30 min	82.2	9.3	5.2	4.2	41
60 min	84.9	9.4	4.2	5.4	45

The process of hydrolyzing BKP in the MALBTH was also monitored by analyzing CHR yield, monosaccharides released, and the degree of polymerization (*DP*) of CHR (Figure 2 and Table 1). Hydrolysis was minor under the swelling condition in LBTH without acid, as confirmed by insignificant *DP* reduction (Table 1) and absence of monosaccharides in the solution (Figure 2B). When acid (5 mM H^+) was added, the cellulose *DP* dropped from 553 to 139 within 10 min. However, over 98% of CHR was still recovered with negligible glucose detected (less than 0.3%), indicating that the acid initiated a significant cutting of cellulose chains but had not yet destroyed fiber structure (Figure 1C) and extensively hydrolyzed cellulose to glucose (Figure 2B). Consequently, the macro-structure of the cellulose fibers stayed intact during the initial hydrolysis stage. Extending the hydrolysis time, the CHR yield gradually decreased from 82.8% at 15 min to 63.1% at 30 min, respectively. Meanwhile, 1.5-5.4% of glucose was released from the hydrolysis of cellulose, and the *DP* of the resultant CHR decreased below 100. No leveling-off degree of polymerization (LODP) was observed as reported by the concentrated acid hydrolysis.[41] At 60 min, only 22.9% CHR was retrieved together with 13.0% glucose. The ~36% total yield of CHR + glucose suggests that a large quantity of aqueous oligosaccharides be generated, possibly due to the homogeneous hydrolysis of cellulose. It is worthy to mention that the LBTH is recyclable and reusable after the MALBTH hydrolysis, although the LBTH recovery is not the main focus here. It was demonstrated that LiBr could be separated and recovered from the hydrolysate using different technologies, such as ion exclusion or exchange chromatography, solvent extraction, and selective crystallization in anti-solvents.[31]

To elucidate the unique hydrolysis behavior of MALBTH, a hydrogen-deuterium exchange

304 experiment was conducted and the accessibility of BKP fibers under the swelling conditions was
305 investigated. Since hydronium ions are readily generated in an aqueous solvent, protons
306 dissociated from a strong acid are assumably as accessible as water molecules in the catalytic
307 hydrolysis of cellulose. In other words, any sites on/in a cellulose microfibril where water can
308 access should be equally accessible to protons. Thus, the region of cellulose accessible to water
309 also represents the hydrolysable portion by acid. Because the hydrogen of hydroxyls exchanges
310 readily with the deuterium in deuterium oxide, the hydroxyls on the accessible cellulose will be
311 labeled via the hydrogen exchange with D_2O molecules in the mildly acidic lithium bromide
312 trideuterate (MALBTD), which could thus be detected by FTIR. As shown in Figure 3, the
313 absorption peaks in the wavenumber ranges of 3200-3600 cm^{-1}, 2800-3000 cm^{-1}, and 2400-2600
314 cm^{-1} were assigned to the vibrational stretching of O-H, C-H, and O-D in cellulose, respectively.[42,
315 43] Compared with the CHR prepared in the MALBTH, these prepared in the MALBTD showed
316 strong vibrational signals of the O-D (Figures 3A-D and S3), indicating occurrence of the
317 hydrogen-deuterium exchange between D_2O and O-H of cellulose. After washing the CHR
318 prepared in MALBTD with H_2O, which could transform the surface O-D back to O-H, the O-D
319 vibrational signals were still detectable, indicating that the certain region of cellulose was
320 inaccessible to H_2O after the exchange. The preserved O-D represented the portion of cellulose
321 (hydroxyls) that was exclusively accessible in MALBTD, but not in the water, as water molecules
322 are only capable of entering the disordered region of cellulose.[42] Therefore, we deduce that the
323 crystalline portion of the cellulose preserved the O-D after the MALBTD treatment. This
324 observation provided direct evidence for our assumption that the H^+/water in the MALBTH could
325 penetrate inside the crystalline region of cellulose under swelling conditions, contributing to the
326 enhanced hydrolysis of cellulose.

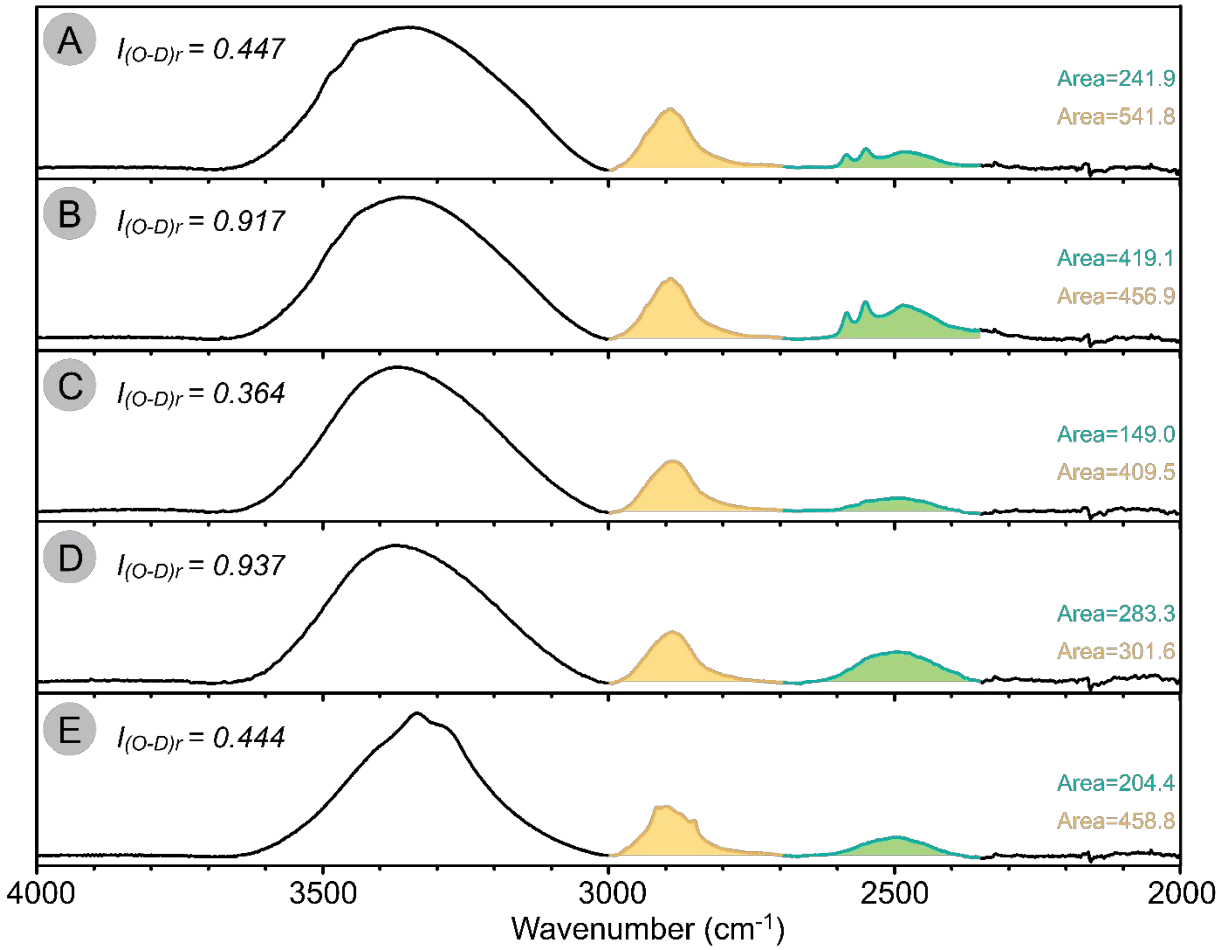

Figure 3. FTIR spectra of cellulose samples from the hydrogen-deuterium exchange experiment. (A. partially hydrolyzed in LiBr·3D_2O for 30 min and washed with H_2O; B. partially hydrolyzed in LiBr·3D_2O for 30 min and washed with D_2O; C. swelled in LiBr·3D_2O for 45 min and washed with H_2O; D. swelled in LiBr·3D_2O for 45 min and washed with D_2O; E. Swelled in D_2O for 45 min and washed with D_2O.) Note: All the treatments were at 100 ℃. A and B were subjected to a swelling process in LiBr·3H_2O and LiBr·3D_2O, respectively before the acid (2.5 mM H_2SO_4) was added. The FTIR spectra were baseline-corrected, normalized and integrated from 3000-2700 cm^{-1} for the C-H vibrational signal and from 2700-2350 cm^{-1} for the O-D vibrational signal. The Y-axis denotes absorption.

As shown in Figure S3 in ESI, hydroxyls (OHs) at C2, C3, and C6 positions of cellulose II were responsible for the three peaks at 3470, 3402, and 3269 cm^{-1}, and deuteroxyls (ODs) at C2, C3, C6 positions of cellulose II were responsible for the three peaks at 2583, 2551, and 2474 cm^{-1}.[40] The relative intensities of the O-D vibrational signals are illustrated in Figure 3 using the C-H

vibrational signal as a reference. Under the mild hydrolysis conditions in the MALBTD, the relative intensities of O-D ($I_{(O\text{-}D)r}$) were 0.447 (counting the hydroxyls in the crystalline region, Figure 3A) and 0.917 (counting all the accessible hydroxyls, Figure 3B). The relative intensity of O-D responsible for the disordered and surface cellulose was calculated to be 0.470. Under the swelling condition in deuterated LBTH without acid, the relative intensities of O-D ($I_{(O\text{-}D)r}$) were 0.573 (for the disordered and surface cellulose) and 0.364 (for the crystalline cellulose). The decreased O-D intensity of the disordered and surface cellulose after hydrolysis in the MLABTD indicated that disordered cellulose was preferentially removed by the selective hydrolysis in the system.

Polymorph transformation of cellulose in the MALBTH and proposed mechanism

The cellulose polymorph in the original BKP was transformed from cellulose I to cellulose II during the treatment in the MALBTH, which were verified by both WAXD and FTIR analyses. As shown in Figure 4A, after the treatment in the MALBTH, the resultant CHR showed diffraction peaks at 12.2° (1-10), 20.0° (110), and 22.1° (020), respectively, which were characteristic for cellulose II crystallites, while the untreated BKP, which is composed of cellulose Iβ crystallites, showed diffraction peaks at 14.8° (110), 16.7° (1-10), and 22.6° (200), respectively. Based on the .cif files provided by French et al.,[34] the ideal XRD patterns were simulated using the generally accepted cellulose Iβ and cellulose II lattice units by the Mercury software, as illustrated in Figures 4B and 4C. The experimental XRD patterns of the original BKP and the CHR prepared in the MALBTH were in perfect agreement with the simulation using ideal cellulose Iβ and cellulose II crystallites, respectively. The results confirmed that the polymorph transformation of cellulose occurred during the MALBTH treatment. Swelling BKP in LBTH without acid resulted in an XRD pattern distinct from cellulose I but consistent with cellulose II (LBTH cellulose in Figure 4A),

366 suggesting that polymorph transformation be initiated under the swelling conditions in the LBTH
367 and completed in the MALBTH. In particular, the diffraction pattern of the CHR after 45 min
368 (Figure 4A) fit well with those of ideal cellulose II (Figure 4C) due to the removal of disordered
369 cellulose. The LBTH or MALBTH treatment was more efficient at transforming cellulose
370 polymorph, compared to other cellulose swelling solvents such as concentrated sulfuric acid and
371 [BMIM]Cl.[11, 25] As far as we are aware, this is the first report of polymorph transformation
372 achieved by swelling cellulose in an aqueous solvent other than corrosive concentrated sodium
373 hydroxide or sulfuric acid.
374

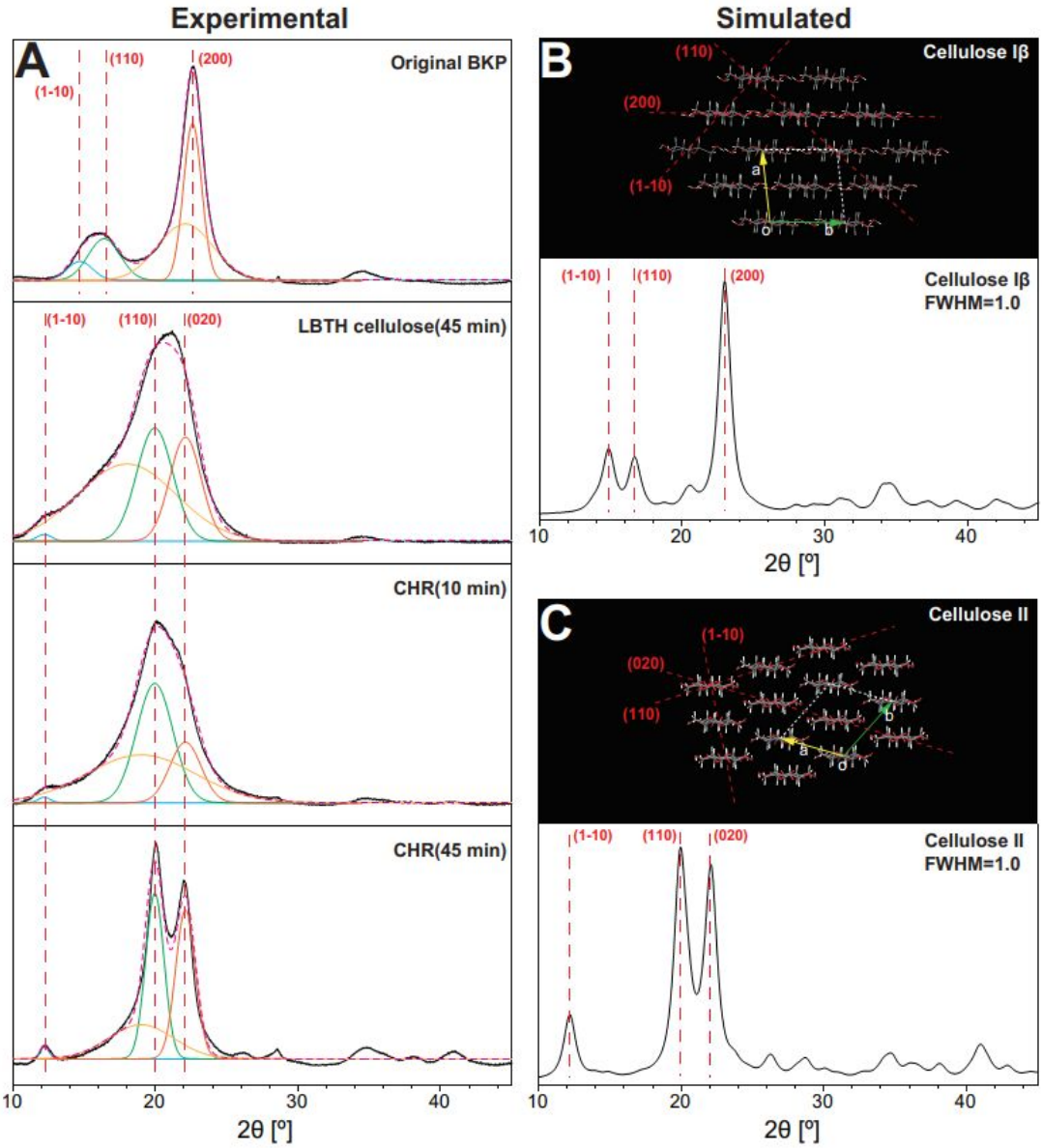

Figure 4. The experimental XRD patterns of BKP and the CHR prepared in the MALBTH (A), the simulated XRD patterns of cellulose Iβ (B), and cellulose II (C).

As shown in Table 1, swelling BKP in the LBTH without acid reduced the crystallinity from 75.1% of original BKP to 62.9% of swelled cellulose II fibers. Reduction in crystallinity is presumably due to the generation of disordered cellulose during polymorph transformation. During the controlled hydrolysis in the MALBTH, the crystallinity of CHR gradually increased with hydrolysis time from 72.3% at 5 min to 90.9% at 45 min because of the removal of disordered

384 cellulose. This confirmed that crystalline cellulose was more recalcitrant to hydrolysis than
385 disordered cellulose. The crystal size corresponding to the three major crystalline planes [(1-10),
386 (110), and (020)] of cellulose II increased by 50-100% when extending the hydrolysis time from
387 5 min to 45-60 min.

388 The transformation from cellulose I to cellulose II was also verified from the FTIR spectra of
389 BKP before and after the treatment in LBTH and MALBTH (Figure S4). The absorption bands at
390 1429, 1105, and 1053 cm^{-1}, which are characteristic for cellulose I (e.g., BKP), disappeared after
391 the treatments in LBTH and MALBTH, verifying again that the polymorph transformation of
392 cellulose was initiated and mostly completed in the LBTH. The vibrational frequency of CH_2
393 symmetric bending shifted to 1418 cm^{-1} from 1429 cm^{-1} in the CHR spectrum, consistent with that
394 of the cellulose II crystallites in lyocell fibers,[44] which is additional evidence of the polymorph
395 transformation from cellulose I to cellulose II in the MALBTH treatment. Furthermore, the
396 enhanced intensity of the vibrational bands at 1368 and 1263 cm^{-1} in the CHR spectrum was
397 consistent with the XRD results above that cellulose II crystallites accumulate as a consequence
398 of polymorph transformation and subsequent hydrolysis of disordered cellulose.
399

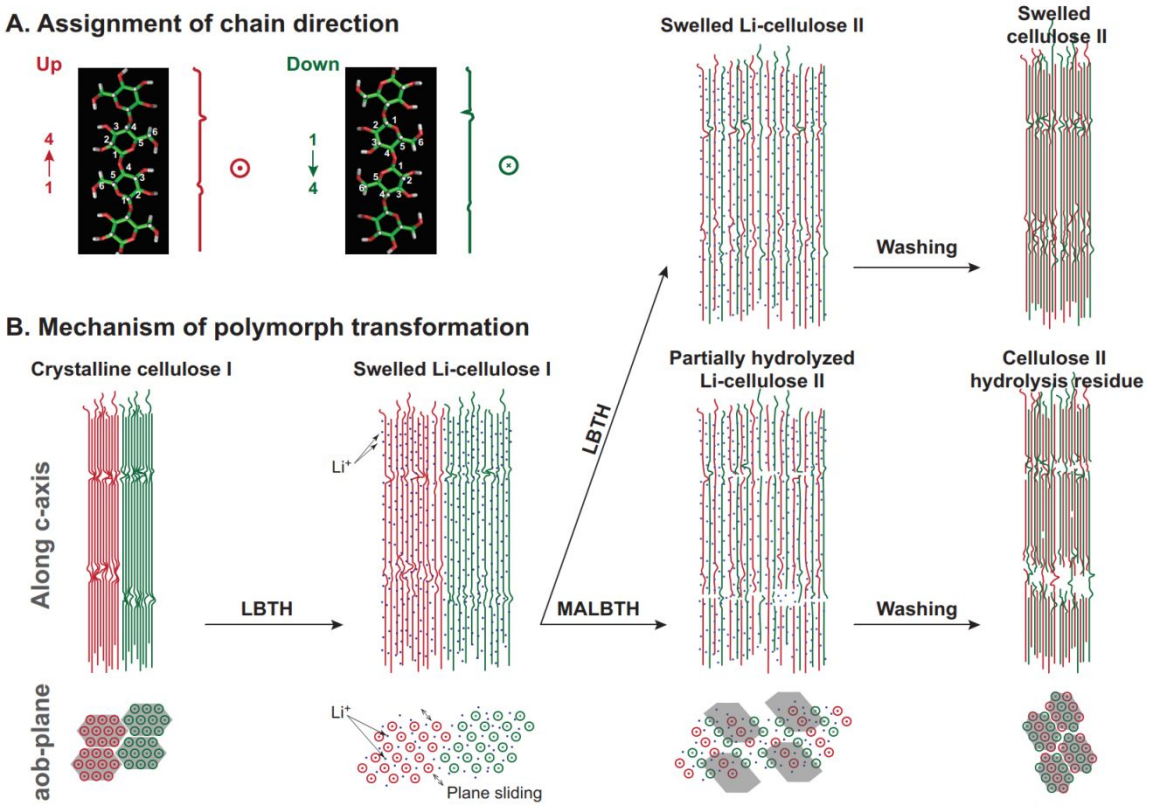

Figure 5. Schematic illustration of the polymorph transformation from cellulose I to cellulose II under swelling conditions in the MALBTH.

An inter-plane transition mechanism was proposed to rationalize the cellulose polymorph transformation in MALBTH under the swelling conditions (Figure 5). At the molecular level, elementary microfibrils in a cellulose fiber are assembled by cellulose chains in a parallel direction.[45] The direction of elementary microfibrils had a random distribution in the cellulose fiber. Either up (red) or down (green) is assigned arbitrarily depending on the relative positions of the C4 and C1 carbons in a glucopyranose unit along the chain axis (Figure 5A).[46] In the LBTH system, hydrated Li^+ can penetrate into the elementary microfibrils (cellulose crystallites) under swelling conditions, partially interrupting the inter-molecular hydrogen bonds between cellulose chains via the ion-dipole coordination with the hydroxyl of cellulose. The hydrated Li^+ in the swelled Li-cellulose I (Figure 5B), acts as a spacer. It disintegrates the microfibril matrix into

414 layers of mobile crystalline planes, which are presumably held together by the inter-chain
415 hydrophobic interactions between the adjacent cellulose of the same chain direction.[47] This is
416 distinct from the cellulose dissolution where all the cellulose chains are fully disintegrated and
417 solvated. Exchanging the crystalline planes between the adjacent microfibril matrixes is feasible
418 due to the dynamic coordination between the hydrated Li^+ and the crystalline planes.[29] It results in
419 an anti-paralleled conformation of cellulose chains cross the planes. The inter-plane transition is a
420 spontaneous process, as the anti-parallel arrangement of cellulose chains is considered to be
421 thermodynamically favorable.[46] When washed with water, the Li^+ ions are removed out of the
422 crystalline cellulose. As a result, the anti-parallel chains of cellulose form new inter-molecular
423 hydrogen bonds between the hydroxyls, resulting in cellulose II crystals after drying.

424 The proposed inter-plane transition mechanism accords with the experimental observation of
425 the polymorph transformation in MALBTH treatment. The re-assembly of the crystalline planes,
426 which slide across cellulose microfibrils, is not perfect, and extra disordered cellulose is formed.
427 This is consistent with the experimental evidence above that the BKP swelled in the LBTH had a
428 lower crystallinity than the original BKP. When subjected to controlled hydrolysis under the
429 swelling conditions, the length of the crystalline planes is shortened by the removal of the
430 disordered cellulose via the hydrolysis. The shorter crystalline planes lead to higher mobility
431 because of reduced spatial hindrance, which further facilitates the polymorph transformation via
432 the crystalline plane sliding between microfibrils. The hypothesis that CHR forms well-organized
433 cellulose crystallites after the inter-plane transition is supported by the experimental results, i.e.,
434 the CHR had an up to 90.9% crystallinity and a large crystallite size: (1-10) 10.1 nm, (110) 5.5
435 nm, and (020) 5.0 nm after 45-min treatment in the MALBTH. Similar mechanisms were also
436 proposed in the mercerization-induced polymorph transformation of cellulose.[46, 48]
437

438 **Disintegration of CHR to ox-CNC II via APS oxidation**

439

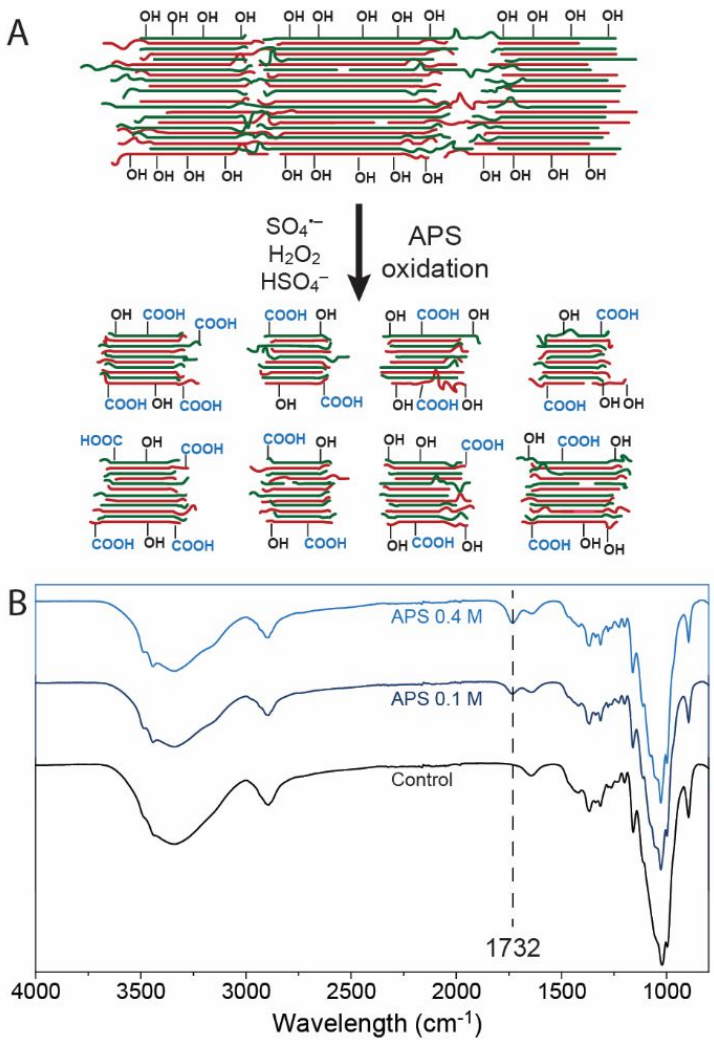

440

441 **Figure 6.** Schematic illustration of the APS oxidation process introducing surface carboxyl on ox-
442 CNC II (A) and the experimental verification by FTIR (B). Note: Control denotes the CHR after
443 30 min MLABTH treatment; APS oxidation conditions: temperature 60 °C, time 12 h.

444

445 To ease the disintegration and dispersion of CNC, a common method is to introduce charges onto
446 the surface of the CNC. In the present study, ammonium persulfate (APS) was used as an oxidizing
447 reagent to introduce carboxyl groups to the surface of the CNC II (CHR) by partial oxidation,
448 which led to the oxidized cellulose II nanocrystals (ox-CNC II) with a negative surface charge. As
449 an alternative to TEMPO reagents, APS can oxidize surface hydroxyls of cellulose nanocrystals

to carboxyl groups but has lower chronic toxicity and cost than TEMPO.[14, 49] At elevated temperatures, persulfate ($S_2O_8^{2-}$) can slowly decompose to $SO_4^{\cdot-}$, HSO_4^-, and H_2O_2. The HSO_4^- provides an acidic environment for further removal of disordered cellulose, and the $SO_4^{\cdot-}$ free radical and H_2O_2 contribute to the oxidation of surface hydroxyl to the carboxyl (Figure 6A). The cellulose residues produced by the swelling alone in the LBTH and the swelling and controlled hydrolysis in the MALBTH were both subjected to the APS oxidation. Starting from the CHR prepared from 15-min treatment in the MALBTH, the maximum yield of the ox-CNC II was 62.1% after the APS oxidation (Table 2). From the swelled BKP in LBTH and the CHR after extensive treatment (30 min) in the MALBTH, the yield of the ox-CNC II was lower under the same APS oxidation conditions (0.1 M APS). The swelling of BKP in the LBTH without acid increased the percentage of overall disordered cellulose, which impeded the release of the high-crystallinity ox-CNC II. As a result, the non-dispersible precipitates with large particle sizes were up to 55.1%, as shown in Figure S5 in ESI. On the other hand, extended hydrolysis in the MALBTH resulted in a significant loss of CHR yield (over 40%), which in turn impaired the final yield of the ox-CNC II calculated based on the initial cellulose content in BKP. The yield of the ox-CNC (23.3%-62.1%, based on BKP, varying with the APS concentration) was comparable to that of the CNC produced by concentrated sulfuric acid (28.0%-75.6%, varying with the sulfuric acid concentration), but lower than that of those produced by TEMPO oxidation (over 90%).[13, 50] The APS oxidation did not affect cellulose polymorph or cause polymorph transformation, as the ox-CNC II maintained the same polymorph as CNC II (Figure S6).

The characteristic peak of the C=O bond at 1732 cm^{-1} in FTIR spectra (Figure 6B) confirmed that carboxyl groups were introduced after the APS oxidation, which oxidized the surface hydroxyl of cellulose into carboxyl. The peak intensity increased with the APS concentration. A semi-

quantitative analysis of the carboxyl content has been reported utilizing FTIR spectra,[49] but the more precise electric conductivity titration method was used to quantitate the carboxyl groups. As shown in Table 2, the carboxyl content increased from 0.4 mmol/$g_{cellulose}$ (0.1 M APS) to 1.2 mmol/$g_{cellulose}$ (0.6 M APS) with the increased APS concentration, indicating concentrated APS greatly enhanced the surface oxidation of cellulose. Introducing carboxyl by APS oxidation is analogous to that by TEMPO oxidation which resulted in 1.1- 1.7 mmol/gcellulose.[48, 49] For comparison, the CNC prepared by concentrated H_2SO_4 was less functionalized (~0.2 mmol/$g_{cellulose}$ sulfate).[50] It is worth noting that the concentration of APS used in this study was significantly lower than that used for other cellulose feedstocks (e.g., lyocell cellulose II fibers and bleached cellulose I pulp) which generally required 1-2 M APS to achieve 1.0 mmol/$g_{cellulsoe}$ carboxyl content on CNC.[49, 51] The low APS concentration requirement in this study is attributed to the enhanced surface accessibility of CHR prepared in the MALBTH. Coupling the swelling and controlled hydrolysis in the MALBTH and the APS oxidation provided a greener and economically favorable option for ox-CNC II production.

Characterization of ox-CNC II

The yield of ox-CNC II is negatively correlated to the APS concentration (Table 2). This is primarily due to the removal of additional disordered cellulose from CNC II (CHR) at high APS concentrations. As no glucose was detected after the APS oxidation, it is speculated that soluble oligo- and mono-glucuronic acids account for the loss of ox-CNC II yield. Increasing the APS concentration contributed to higher *CrI*, indicating that the disorder cellulose (ether the original disordered section or the regenerated paracrystalline cellulose) was selectively removed. When the APS concentration was above 0.2 M, the crystallinity of the ox-CNCs II reached up to ~95%, based on the Segal method, as a result of the extensive removal of disordered cellulose (Table 2).

Because the Segal method regulated the disordered intensity of cellulose II at 2θ 16° for the *CrI* calculation, resulting in underestimation of the disordered cellulose II,[15] the relative crystallinity of cellulose was calculated using the deconvolution method (*CrI′*) as well for comparison. The *CrI and CrI′* values calculated by the two methods follow the same trend (Table 2). The *CrI′* of cellulose II also reached over 85% for the APS-oxidized samples. The crystallinity indices calculated by the Segal and the deconvoluted methods both verified the ultra-high crystallinity of the ox-CNC II.

The hydrodynamic diameter of the ox-CNC II was estimated by DLS analysis for comparing relative size among the samples prepared under different APS oxidation conditions. It must be noted that the diameter value, as fitted by isotropic particles, does not represent the real dimension of rod-like nanoparticles.[48] For the CHR prepared after treatment in the MALBTH for 15 min, the hydrodynamic diameters of the resultant ox-CNC II decreased from 208 to 80 nm when increasing the APS concentration from 0.1 to 0.6 M, as shown in Table 2. The effect of the APS oxidation duration was insignificant on the relative size of the ox-CNC II, especially after 12 h. However, extending the hydrolysis in the MALBTH could reduce the hydrodynamic diameter of the ox-CNC II to smaller than 60 nm after the oxidation with 0.4 M APS.

Table 2 Effects of APS oxidation on yield, crystallinity indices (*CrI* and *CrI′*), carboxyl content, hydrodynamic diameter, and zeta potential of ox-CNC II

MALBTH hydrolysis (min)	APS (M)	APS duration (h)	Yield[a] (%)	*CrI* / *CrI′* (%)	Carboxyl content (mmol/g)	Particle size (nm)[c]	Zeta potential (mV)
0 (Swelling)	0.1	12	39.7 (55.1)	82.9 / 58.5	- -[b]	417	-32
	0.2	12	57.3 (24.9)	85.6 / 59.2	- -	374	-44
	0.4	12	55.2 (2.0)	86.9 / 62.8	- -	132	-40
15	0.1	12	62.1	87.4 / 59.6	0.40	208	-49
	0.2	8	54.7	95.0 / 69.8	0.44	207	-48
	0.2	12	51.5	96.3 / 71.9	0.44	200	-53
	0.2	18	41.8	96.2 / 72.4	0.50	211	-54

	0.4	12	38.4	98.4 / 79.2	0.59	147	-53
	0.6	12	23.3	99.6 / 85.3	0.92	80	-59
	0.1	6	55.2	92.9 / 66.3	0.42	179	-38
	0.1	12	52.6	95.2 / 69.6	0.41	164	-43
	0.2	6	48.4	94.3 / 72.4	0.36	136	-45
30	0.2	12	43.2	96.4 / 80.1	0.43	98	-45
	0.2	18	39.9	95.5 / 79.3	0.49	93	-48
	0.4	12	24.6	97.7 / 85.9	0.57	57	-52
	0.6	12	10.1	97.4 / 87.0	1.20	85	-45

a. The yield is based on the initial cellulose content in BKP; the value in the parenthesis denotes the yield of un-dispersible precipitate after oxidation;
b. The carboxyl content analysis was not conducted for the LBTH swelled samples;
c. The relative particle size (the hydrodynamic diameter of ox-CNC II) was obtained by DLS analysis.

APS oxidation of BKP generated the ox-CNC I without polymorph transformation. A needle-like shape with sharp endings (Figure 7A) was observed with an averaged length 151 ± 51 nm and an average width 9.8 ± 2.4 nm (Figure 7D and 7G). The ox-CNC II from the MALBTH treated CHR had a rod-like shape with blunt endings (Figures 7B and 7C). The shape of the ox-CNC II was similar to the CNC II prepared by the extensive hydrolysis in concentrated sulfuric acid, but different from that of the cellulose I CNC.[52] The averaged length and width of ox-CNC II (0.2 M APS) were 57 ± 24 nm and 9.3 ± 3.1 nm, respectively (Figure 7E and 7H). Increasing the APS concentration reduced the longitudinal dimension to 26 ± 11 nm (Figure 7F) but did not affect the width dimension (9.9 ± 3.6 nm) (Figure 7I). The thickness parameter of ox-CNC II was 8.0-8.5 nm, estimated by AFM (Figure S7 in ESI), confirming that the lateral dimension was relatively constant in the APS oxidation. As a result, the ox-CNC II could have a tunable aspect ratio by varying APS oxidation conditions.

Divergent from the CNC I prepared from wood pulps by APS oxidation (L: 151 nm, W: 9.8 nm) and concentrated sulfuric acid (L:105-147 nm, W: 4.5-5.0 nm),[53] the ox-CNC II were much shorter in length (26-57 nm). This unique dimensional feature was ascribed to the polymorph

transformation under swelling conditions in the MALBTH treatment. The polymorph transformation of BKP in MALBTH involved the re-assembly of cellulose crystallites via an inter-plane transition. Extending the hydrolysis time generated larger crystallites with a lower DP (Table 1). It differed from the cellulose hydrolysis without polymorph transformation in which the crystallite size was relatively constant.[54] Besides, the APS oxidation of CHR did not change the width dimension of ox-CNC II (Figure 7). The results above suggest that the CHR had the fringed-micellar structure in which additional disordered cellulose was generated from the inter-plane transition process, contributing to the tailorable aspect ratio of ox-CNC II. For comparison, the CNC II prepared in an ionic liquid ([BMIM]Cl) via a dissolution and regeneration process had irregular and mixed shape and size, including rod-shape CNC II (L: 112 nm, W: 12 nm) and sphere-shape CNC II (118 nm in diameter).[25]

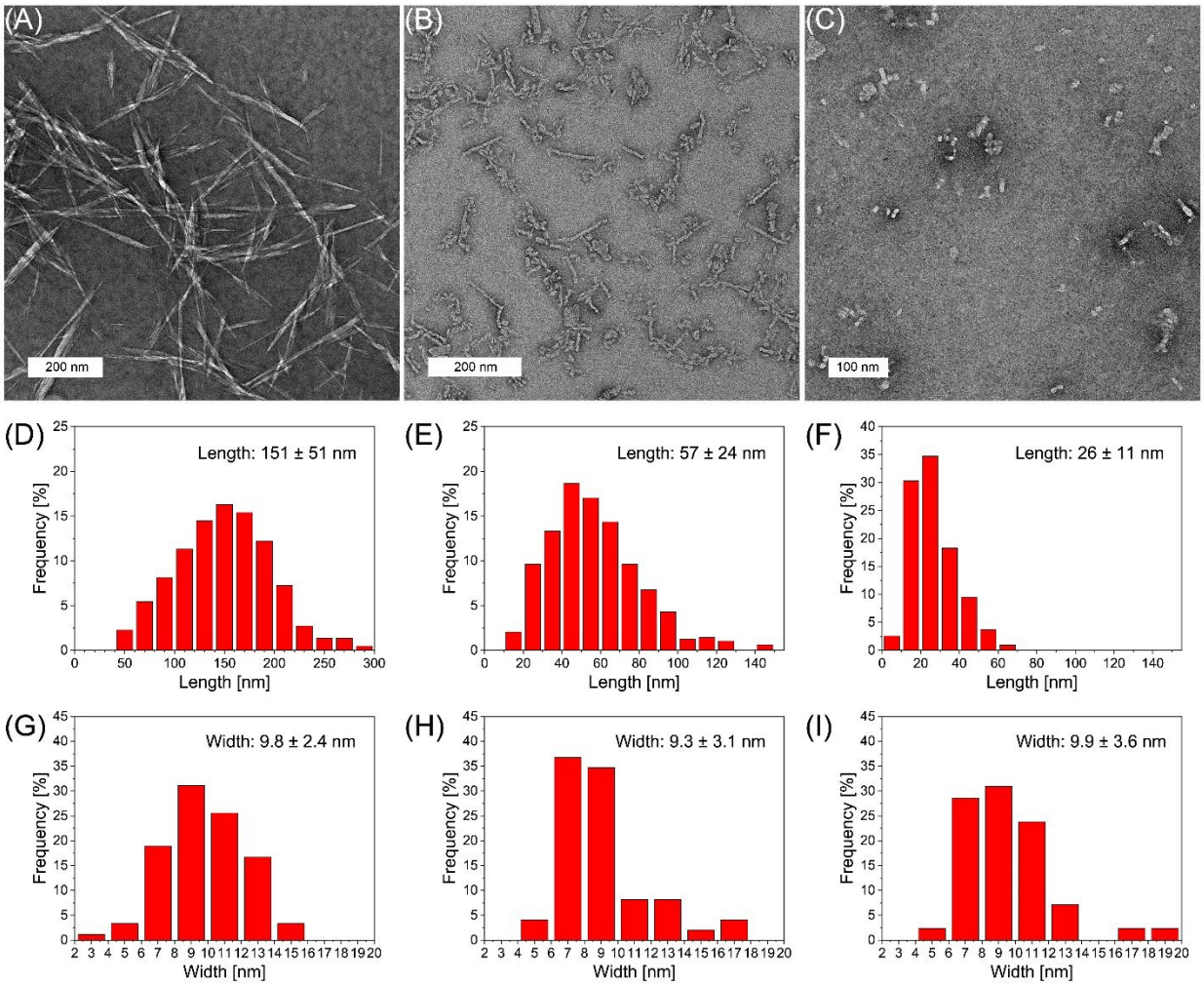

Figure 7. TEM images and dimensional distributions of ox-CNC I from BKP treated with 0.8 M APS (A, D, and G); ox-CNC II from CHR (15 min MALBTH treatment) treated with 0.2 M APS (B, E, and H); ox-CNC II from CHR (15 min MALBTH treatment) treated with 0.6 M APS (C, F, and I). APS oxidation conditions: temperature 60 °C, oxidation time 12 h.

The ox-CNC II exhibited high zeta potential ranging from -42.8 to -59.0 mV, depending on the carboxyl content and the particle size of the ox-CNC II prepared under varied oxidation conditions (Table 2). The zeta potential was relevant to surface charge density which was calculated using the dimensions determined by TEM and AFM, considering ox-CNC II with rod-shape and cellulose density 1.6 g/cm^3. Full dissociation of carboxyl was assumed at the neutral pH. The surface charge density of ox-CNC II increased from 0.87 e$^-$/nm^2 (0.2 M APS) to 1.72 e$^-$/nm^2 (0.6 M APS), while the average crystallite size was relatively stable (6.2 nm and 6.8 nm, respectively).

It differed from the TEMPO-oxidized CNC which showed the decreased the carboxylate density with the crystalline size.[55] At 0.6 M APS, the surface charge density of ox-CNC II was comparable to that of CNC by the TEMPO (~1.7 group/ nm^2) and higher than that by the concentrated H_2SO_4 (0.29-0.38 e^-/nm^2).[55, 56] The high zeta potential (absolute value) would grant ox-CNC II excellent colloidal stability in water. The colloid suspension (0.5-1.0 wt%) of the ox-CNC II prepared under varied APS oxidation conditions was found to be stable for up to 6 months, as shown in Figure S8 in ESI. In contrast, flocculation was inevitable for traditional CNC after weeks of storage.[57]

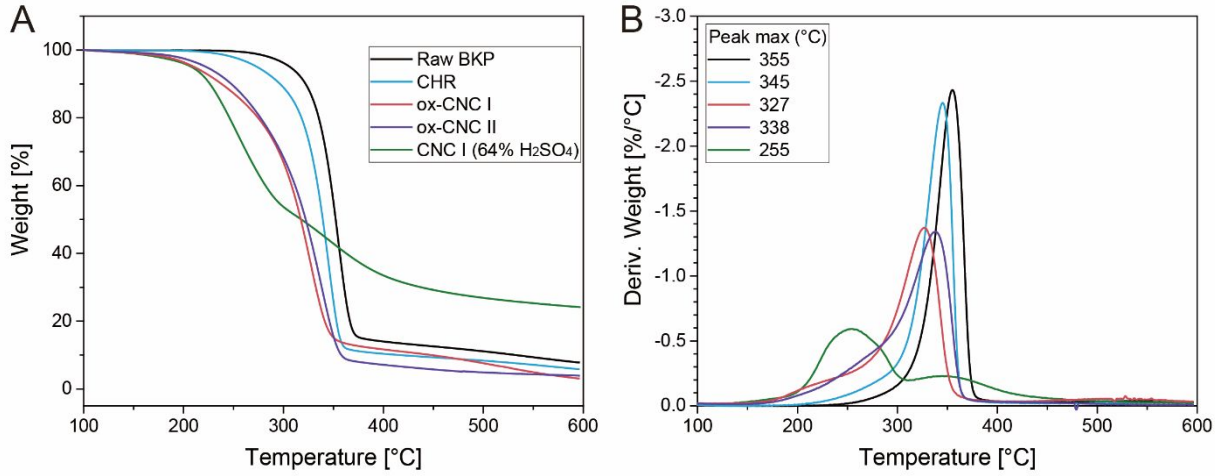

Figure 8. TGA and the first derivative curves of various cellulose samples.

The thermal stability of cellulose samples with different cellulose polymorphs was evaluated using TGA (Figure 8). The ox-CNC II from the MALBTH treated CHR had the major pyrolytic degradation peak at 338 °C which was slightly lower than those of original BKP (355 °C) and CHR (345 °C). The slight decrease in thermal stability was ascribed to the reduced molecular weight of the ox-CNC II caused by the hydrolysis in the MALBTH and the introduced carboxyl groups by the APS oxidation. Compared with the ox-CNC II, the ox-CNC I without the MALBTH treatment had lower stability at temperatures above 300 ºC. This is consistent with the hypothesis

that thermodynamically, cellulose II is more resistant to thermal degradation than cellulose I.[58] Traditional CNC I prepared by the controlled hydrolysis in 64% H_2SO_4 displayed a downward shift in its major degradation peak (255 °C), indicating a significant decrease in thermal stability. The results above confirmed the ox-CNC II derived from the MALBTH CHR had improved thermal stability.

Conclusions

The simultaneous hydrolysis and polymorph transformation of cellulose I fibers (BKP) in the MALBTH followed by the APS oxidation was successfully demonstrated for preparing cellulose II nanocrystals. The hydrated lithium ions (Li^+) in the MALBTH swelled the cellulose fibers via disrupting the intermolecular hydrogen bonds of cellulose. The removal of the disordered cellulose by selective hydrolysis in the MALBTH under the swelling condition resulted in well-organized crystallites. Meanwhile, it was proven that the lithium ions were able to penetrate inside the cellulose crystallites under the swelling condition using the hydrogen-deuterium exchange experiment, which led to the sliding and reassembling of the crystalline planes of cellulose and thereby caused the polymorph transformation from parallel-oriented cellulose I to anti-parallel-oriented cellulose II. The APS oxidation at low APS concentrations (0.1-0.6 M) introduced the surface charges (0.3-1.2 mmol $COOH/g_{cellulose}$) and therefore facilitated the disintegration of the cellulose nanocrystals. The yield of the ox-CNC II was up to 62%. The resultant ox-CNC II featured ultra-high crystallinity (above 90%), excellent dispersibility and colloidal stability, and good thermal stability. Depending on the conditions of the MALBTH hydrolysis and APS oxidation, the length of the ox-CNC II was tunable (26-57 nm) with a relatively constant lateral dimension (8-10 nm). This study provides a caustic-chemical-free method to produce tunable

cellulose II nanocrystals by the simultaneous hydrolysis and polymorph transformation of cellulose I in the MALBTH system.

Acknowledgments: This work was supported by the National Science Foundation (NSF) (CBET 1159561) and the U.S. Department of Agricultural (USDA) National Institute of Food and Agriculture, McIntire Stennis grant (WIS01996) to XP. NL is thankful to China Scholarship Council (CSC) for partially supporting his Ph.D. study at the University of Wisconsin-Madison.

Author contributions: NL and XP conceived the idea and designed the research. NL conducted most of the experiments, and HB finished the AFM analysis. TEM imaging was performed by PNC and NL. NL, HB, XP, JZ, and PNC analyzed the data. NL and XP drafted the manuscript. All authors reviewed the manuscript and suggested improvements.

Competing interests: All authors declare no conflict of interest.

References

1. D. Klemm, B. Heublein, H. P. Fink and A. Bohn, *Angewandte Chemie,* 2005, **44**, 3358-3393.
2. H. Zhu, W. Luo, P. N. Ciesielski, Z. Fang, J. Y. Zhu, G. Henriksson, M. E. Himmel and L. Hu, *Chemical Reviews*, 2016, **116**, 9305-9374.
3. O. M. Vanderfleet and E. D. Cranston, *Nature Reviews Materials*, 2020, 1-21.
4. D. Trache, M. H. Hussin, M. M. Haafiz and V. K. Thakur, *Nanoscale*, 2017, **9**, 1763-1786.
5. S. Wang, A. Lu and L. Zhang, *Progress in Polymer Science*, 2016, **53**, 169-206.
6. A. Dufresne, *Materials Today*, 2013, **16**, 220-227.
7. B. L. Tardy, S. Yokota, M. Ago, W. Xiang, T. Kondo, R. Bordes and O. J. Rojas, *Current Opinion in Colloid & Interface Science*, 2017, **29**, 57-67.
8. N. Grishkewich, N. Mohammed, J. Tang and K. C. Tam, *Current Opinion in Colloid & Interface Science*, 2017, **29**, 32-45.
9. X. Wang, C. Yao, F. Wang and Z. Li, *Small*, 2017, **13**, 1702240.
10. C. Miao and W. Y. Hamad, *Current Opinion in Solid State and Materials Science*, 2019, **23**, 100761.
11. D. Bondeson, A. Mathew and K. Oksman, *Cellulose*, 2006, **13**, 171-180.

12. W. Y. Hamad and T. Q. Hu, *The Canadian Journal of Chemical Engineering*, 2010, **88**, 392-402.
13. L. Chen, Q. Wang, K. Hirth, C. Baez, U. P. Agarwal and J. Zhu, *Cellulose*, 2015, **22**, 1753-1762.
14. A. C. Leung, S. Hrapovic, E. Lam, Y. Liu, K. B. Male, K. A. Mahmoud and J. H. Luong, *Small*, 2011, **7**, 302-305.
15. S. Nam, A. D. French, B. D. Condon and M. Concha, *Carbohydrate Polymers*, 2016, **135**, 1-9.
16. L. Chen, J. Zhu, C. Baez, P. Kitin and T. Elder, *Green Chemistry*, 2016, **18**, 3835-3843.
17. H. Yu, Z. Qin, B. Liang, N. Liu, Z. Zhou and L. Chen, *Journal of Materials Chemistry A*, 2013, **1**, 3938-3944.
18. S. Camarero Espinosa, T. Kuhnt, E. J. Foster and C. Weder, *Biomacromolecules*, 2013, **14**, 1223-1230.
19. I. Kalashnikova, H. Bizot, P. Bertoncini, B. Cathala and I. Capron, *Soft Matter*, 2013, **9**, 952-959.
20. I. Capron, O. J. Rojas and R. Bordes, *Current Opinion in Colloid & Interface Science*, 2017, **29**, 83-95.
21. J. M. González-Domínguez, A. Ansón-Casaos, L. Grasa, L. Abenia, A. Salvador, E. Colom, J. E. Mesonero, J. E. García-Bordejé, A. M. Benito and W. K. Maser, *Biomacromolecules*, 2019, **20**, 3147-3160.
22. Y. Qin, X. Qiu and J. Zhu, *Scientific Reports*, 2016, **6**, 35602.
23. M. Hirota, N. Tamura, T. Saito and A. Isogai, *Cellulose*, 2012, **19**, 435-442.
24. M. Beaumont, T. Nypelö, J. König, R. Zirbs, M. Opietnik, A. Potthast and T. Rosenau, *Greem Chemistry*, 2016, **18**, 1465-1468.
25. J. Han, C. Zhou, A. D. French, G. Han and Q. Wu, *Carbohydrate Polymers*, 2013, **94**, 773-781.
26. G. Sebe, F. Ham-Pichavant, E. Ibarboure, A. L. Koffi and P. Tingaut, *Biomacromolecules*, 2012, **13**, 570-578.
27. Y.-J. Yang, J.-M. Shin, T. H. Kang, S. Kimura, M. Wada and U.-J. Kim, *Cellulose*, 2014, **21**, 1175-1181.
28. X. Zhang, N. Xiao, H. Wang, C. Liu and X. Pan, *Polymers*, 2018, **10**, 614.
29. Y. Liao, Z. Pang and X. Pan, *ACS Sustainable Chemistry & Engineering*, 2019, **7**, 17723-17736.
30. L. Zhang, Y. Liao, Y. C. Wang, S. Zhang, W. Yang, X. Pan and Z. L. Wang, *Advanced Functional Materials*, 2020, 2001763.
31. X. Pan and L. Shuai, Saccharification of lignocellulosic biomass. US Patent 9,187,790B2, 2015.
32. L. Shuai, Q. Yang, J. Zhu, F. Lu, P. Weimer, J. Ralph and X. Pan, *Bioresource Technology*, 2010, **101**, 3106-3114.
33. C. F. Macrae, I. J. Bruno, J. A. Chisholm, P. R. Edgington, P. McCabe, E. Pidcock, L. Rodriguez-Monge, R. Taylor, J. v. Streek and P. A. Wood, *Journal of Applied Crystallography*, 2008, **41**, 466-470.
34. A. D. French, *Cellulose*, 2014, **21**, 885-896.
35. W. P. F. Neto, J.-L. Putaux, M. Mariano, Y. Ogawa, H. Otaguro, D. Pasquini and A. Dufresne, *RSC Advances*, 2016, **6**, 76017-76027.
36. N. Li, X. Pan and J. Alexander, *Green Chemistry*, 2016, **18**, 5367-5376.

37. H. Wang, D. Li, H. Yano and K. Abe, *Cellulose*, 2014, **21**, 1505-1515.
38. W. Wang, M. D. Mozuch, R. C. Sabo, P. Kersten, J. Zhu and Y. Jin, *Cellulose*, 2015, **22**, 351-361.
39. A. A. Oun and J.-W. Rhim, *Carbohydrate Polymers*, 2016, **150**, 187-200.
40. Y.-H. P. Zhang, J. Cui, L. R. Lynd and L. R. Kuang, *Biomacromolecules*, 2006, **7**, 644-648.
41. Y. Nishiyama, U.-J. Kim, D.-Y. Kim, K. S. Katsumata, R. P. May and P. Langan, *Biomacromolecules*, 2003, **4**, 1013-1017.
42. E. L. Lindh and L. Salmén, *Cellulose*, 2017, **24**, 21-33.
43. J. Fan, M. De Bruyn, V. L. Budarin, M. J. Gronnow, P. S. Shuttleworth, S. Breeden, D. J. Macquarrie and J. H. Clark, *Journal of the American Chemical Society*, 2013, **135**, 11728-11731.
44. F. Carrillo, X. Colom, J. Sunol and J. Saurina, *European Polymer Journal*, 2004, **40**, 2229-2234.
45. Y. Nishiyama, P. Langan and H. Chanzy, *Journal of the American Chemical Society*, 2002, **124**, 9074-9082.
46. T. Okano and A. Sarko, *Journal of Applied Polymer Science*, 1985, **30**, 325-332.
47. B. Lindman, B. Medronho, L. Alves, C. Costa, H. Edlund and M. Norgren, *Physical Chemistry Chemical Physics*, 2017, **19**, 23704-23718.
48. T. Okano and A. Sarko, *Journal of Applied Polymer Science*, 1984, **29**, 4175-4182.
49. M. Cheng, Z. Qin, Y. Liu, Y. Qin, T. Li, L. Chen and M. Zhu, *J. Mater. Chem. A*, 2014, **2**, 251-258.
50. A. Rattaz, S. P. Mishra, B. Chabot and C. Daneault, *Cellulose*, 2011, **18**, 585-593.
51. K. Zhang, P. Sun, H. Liu, S. Shang, J. Song and D. Wang, *Carbohydrate Polymers*, 2016, **138**, 237-243.
52. W. P. Flauzino Neto, J.-L. Putaux, M. Mariano, Y. Ogawa, H. Otaguro, D. Pasquini and A. Dufresne, *RSC Adv.*, 2016, **6**, 76017-76027.
53. S. Beck-Candanedo, M. Roman and D. G. Gray, *Biomacromolecules*, 2005, **6**, 1048-1054.
54. C. Driemeier and J. Bragatto, *The Journal of Physical Chemistry B*, 2013, **117**, 415-421.
55. Y. Okita, T. Saito and A. Isogai, *Biomacromolecules*, 2010, **11**, 1696-1700.
56. S. Beck-Candanedo, M. Roman and D. G. Gray, *Biomacromolecules*, 2005, **6**, 1048-1054.
57. J. Lazko, T. Sénéchal, N. Landercy, L. Dangreau, J.-M. Raquez and P. Dubois, *Cellulose*, 2014, **21**, 4195-4207.
58. Y. Yue, C. Zhou, A. D. French, G. Xia, G. Han, Q. Wang and Q. Wu, *Cellulose*, 2012, **19**, 1173-1187.